INFLUENCE OF WORKPIECE TEMPERATURE ON PROCESS FORCES AND MACHINING STABILITY

SIMON JAQUET[1, *], DIRK BIERMANN[1]

[1]Institute of Machining Technology (ISF), TU Dortmund University, Dortmund, Germany

DOI: 10.17973/MMSJ.2026_11_2026058

e-mail: simon.jaquet@tu-dortmund.de

Machining thin-walled components often suffers from dynamic instabilities like chatter due to low structural rigidity. While cryogenic support structures formed by expanding liquid CO_2 and a lubricant provide a promising stabilisation method, they introduce complex dynamic trade-offs. Specifically, sub-zero temperatures elevate workpiece material strength, leading to higher process excitation forces. Concurrently, the cryogenic cooling and ice layer shift the natural frequencies, enhancing structural stiffness. This study evaluates the critical balance between these increased excitation forces and the enhanced structural rigidity. Utilising a geometric-physical process simulation, the competing temperature-dependent effects on machining dynamics are comprehensively analysed. The results quantify how this trade-off dictates process stability, offering a predictive framework for process planning. Consequently, this work enables precise stability assessments for cryogenic-assisted thin-walled milling.

KEYWORDS

Process dynamics, cutting fundamentals, ice-based fixtures, cutting-forces, simulation

1 INTRODUCTION

Thin-walled aerospace structures are widely used to reduce component weight while maintaining sufficient mechanical strength [Zhu et al. 2018]. Since often more than 90 % of the material is removed by milling [Herranz et al. 2005], the manufacturing of these parts is dominated by subtractive processes that must account with the inherently low structural stiffness of the finished geometry. This low rigidity makes thin-walled components highly prone to static deflection and dynamic instabilities such as regenerative chatter, which directly compromise dimensional accuracy and surface quality [Quintana and Ciurana 2011]. Among the established chatter-suppression strategies, increasing the structural rigidity of the workpiece through additional or temporary support and enhancing the damping capacity are considered particularly effective for vibrations originating from the workpiece itself [Munoa et al. 2016]. Fixturing and clamping-based approaches have therefore been the subject of extensive research [Möhring et al. 2025]. Cryogenically generated ice layers represent a comparatively recent addition to this class of methods. By expanding liquid CO_2 and injecting a coolant-lubricant emulsion onto the workpiece surface, a temporary support structure is formed that simultaneously stiffens and damps the thin-walled section without requiring the manual installation and removal associated with conventional auxiliary fixtures [Jaquet et al. 2026]. Related concepts based on complete freezing of the workpiece have likewise been shown to suppress machining-induced deformation and to improve dimensional accuracy and surface quality in the milling of thin-walled and cantilevered parts [Wang et al. 2025; Liu et al. 2021]. The feasibility of the jet-based approach used in the present work was first demonstrated in [Jaeger et al. 2020], and a systematic experimental evaluation of its stabilizing effect and the associated thermal distortion was recently reported [Jaquet et al. 2026]. While these studies confirm that cryogenic cooling can substantially increase the dynamic stiffness of a thin-walled workpiece, they also point to a competing effect that has so far received little attention: the sub-zero temperatures induced by the CO_2 lubricant jet not only stiffen the structure but also alter the mechanical properties of the workpiece material itself. It is well established that decreasing temperature raises the yield strength and flow stress of metallic materials. In cryogenic and liquid-nitrogen-assisted machining this has repeatedly been found to increase cutting or milling forces compared with dry or wet machining [Bian et al. 2025], even where cryogenic cooling simultaneously improves tool life and surface finish [Korkmaz and Gupta 2024]. A comparable strengthening has been reported for aluminium alloys, whose yield stress and tensile strength can increase markedly at cryogenic temperatures [Jin et al. 2024], and cryogenic cooling has recently also been investigated for the EN AW-7075 alloy used in the present study, though so far mainly with regard to thermal and surface-related effects [Ranjbar et al. 2026]. The opposite relationship is observed in thermally assisted machining, where locally heating the workpiece ahead of the tool reduces its yield strength and thereby lowers the resulting process forces, an effect that has previously been investigated [Platt et al. 2020]. In parallel, the sub-zero temperatures increase the elastic modulus of the workpiece material: for aluminium alloys, elastic stiffness has been reported to rise by up to 4-13 % upon cooling from room temperature to cryogenic conditions [Naimon et al. 1975], an effect that adds to the geometric reinforcement provided by the adhering ice layer itself.

The application of cryogenic support structures to thin-walled milling therefore involves two opposing, temperature-dependent mechanisms: an increase in structural stiffness and damping, which is beneficial for process stability, and a simultaneous increase in the process excitation force resulting from the higher flow stress of the cooled workpiece material. Since both effects scale with the same process parameter, the workpiece temperature, a systematic separation and quantification of their individual contributions to the machining dynamics is required in order to predict under which conditions the stabilizing effect of the ice layer outweighs the increase in excitation force. Purely experimental investigations, including the authors' own prior work, are limited in their ability to isolate these two mechanically coupled effects, since force and stiffness change simultaneously with the applied cooling strategy.

To close this gap, the present study employs a geometric-physical process simulation in which the temperature-dependent excitation force and the temperature dependent structural stiffness of the workpiece are varied independently. This allows the competing effects to be quantified separately and analysed with respect to their combined influence on process stability. Section 2 describes the experimental setup and the simulation methodology, Section 3 presents and discusses the resulting modal, force and stability data, and Section 4 concludes the paper.

2 CONSTRUCTION OF THE EXPERIMENTAL SETUP

To separate the two competing, temperature dependent effects, this section describes the experimental and simulative framework used in this study. Section 2.1 presents the experimental modal analysis (EMA) used to quantify the

temperature-dependent structural stiffness and damping, Section 2.2 describes the force measurements used to quantify the temperature-dependent excitation force, and Section 2.3 outlines how both data sets are combined in a geometric-physically based process simulation to predict process stability.

2.1 Modal Analysis

A setup similar to the one used in [Jaquet et al. 2026] was employed to control the workpiece temperature during the experimental modal analysis (EMA). In contrast, however, only the CO_2 jet was applied in these tests, without the additional injection of the coolant–lubricant emulsion. Consequently, no ice-based support structure formed on the workpiece surface, and only the effect of the sub-zero workpiece temperature on the structural dynamics was investigated, decoupled from any additional geometric reinforcement by an ice layer (Figure 1). The sub-zero CO_2 jet is generated via Joule–Thomson expansion of liquid CO_2, exiting the nozzle (d_{Nozzle} = 1.7 mm) at approximately T = −79 °C and a standoff distance of a_{Nozzle} = 70 mm, directed perpendicular to the blade surface. All measurement equipment is mounted on the rear face of the workpiece to shield it from the cryogenic flow. Structural excitation is performed with an automated impact hammer (vImpact-62, Maul-Theet) mounted on a linear stage. It remains retracted during CO_2 application and is advanced into its operating position only immediately before the EMA measurements. The resulting deflections are captured with an eddy-current displacement sensor (eddyNCDT 3061, Micro-Epsilon; standoff and measuring range of 0.3 mm), whose integrated temperature compensation was benchmarked against laser measurements beforehand. The workpiece temperature is monitored with a type-N thermocouple, applied with thermal paste at the base of the component to minimize contact resistance. The test specimen was manufactured from EN AW-7075 T6 and consisted of a base section with a cantilevered thin-walled blade (t = 3 mm, h_w = 40 mm, w = 55 mm). The FRF was measured at a height of h_s = 35 mm above the base and at a distance of 5 mm from the edge of the wall. This off-centre position was selected deliberately so that both the bending and the torsional modes of the blade are excited and captured. A measurement at the wall centre would not have resolved the torsional modes, which govern the response at the outer regions of the wall. Since a temperature sensor attached directly to the thin wall would locally alter its mass and stiffness and interfere with the free oscillation to be measured, the workpiece temperature was monitored at the base. A minimum equalisation time of 10 s was maintained between the end of the CO_2 application and the first FRF measurement. Owing to the high thermal conductivity of the aluminium alloy, the temperature field equalises rapidly within this period, which was verified by transient thermal FE simulations (ANSYS) for both component geometries. A residual offset between base and wall acts systematically across all temperature levels, as jet configuration, standoff distance and application time were identical in every test, and therefore should not affect the relative temperature-dependent trends evaluated here. Each test condition was performed twice. For every measurement point the blade was excited by five hammer impacts, separated by at least 2 s to ensure complete decay of vibration, and the resulting frequency response function (FRF) was computed from the five measurements using an H1 estimator, with coherence used to assess measurement quality.

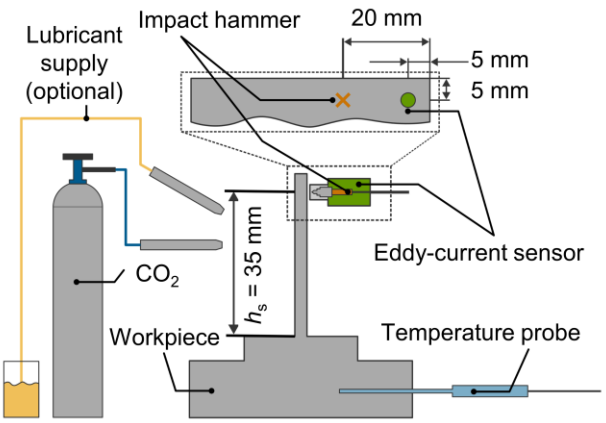


Figure 1. Experimental setup EMA.

2.2 Force Measurement

For the force measurements, an aluminium specimen of the workpiece material EN-AW 7075 T6 was mounted on a piezoelectric dynamometer (type 9257B, Kistler) and thermally decoupled from the platform by ceramic base plates (Figure 2). The workpiece was cooled with the CO_2 jet to approximately 5 °C below the intended target temperature. Cooling was then stopped and the specimen was allowed to warm to the target temperature through natural heat exchange with the ambient air prior to machining, ensuring a homogeneous temperature distribution before each cut. Milling tests were carried out at a spindle speed of n = 5000 min^{-1}, which equals to a cutting speed of $v_c \approx$ 125.7 m/min, with a radial depth of cut a_e = 3 mm, an axial depth of cut a_p = 5 mm and a feed per tooth of f_z = 0.1 mm, using a two-fluted end mill (Gühring, type 3452, d = 8 mm). To remove the dynamic response of the measurement chain from the recorded force signal, an inverse filter was applied. The transfer function G_{FF} of the fully assembled measurement chain, comprising specimen, ceramic base plates and dynamometer, was determined experimentally by exciting the structure with an impulse hammer (type 8206, Brüel & Kjær) at a representative mean force application point, successively in all three spatial directions. Hammer excitation and dynamometer response were recorded simultaneously, and G_{FF} was computed as their ratio in the frequency domain. Each temperature level was measured in two independent experiments. To avoid superimposing position-dependent effects on the temperature dependence under investigation, the test sequence was randomised with respect to machining position, so that no two consecutive tool paths were machined at the same workpiece temperature.

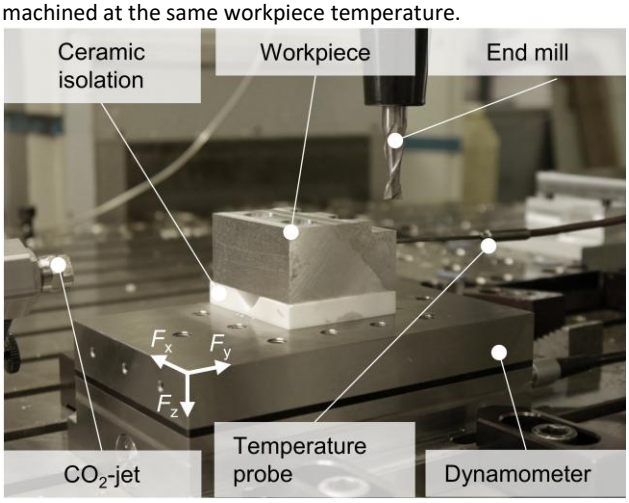


Figure 2. Experimental setup force measurement.

2.3 Simulation

A geometric-physically based process simulation [Wiederkehr et al. 2018] was employed to predict the machining stability for the investigated operating conditions. The modal parameters mass, stiffness and damping, obtained from the EMA described in Section 2.1, were used as the dynamic input for the stability calculation. A nonlinear empirical force model was [Kienzle 1952] applied to predict the resulting process forces. It is particularly suitable for modelling the forces in machining processes with interrupted cuts such as milling. In this model, the undeformed chip thickness h_{cu} and the segment width w of the considered cutting edge are used to determine the resulting forces

$$\boldsymbol{F_i = w \cdot k_i \cdot h_0 \cdot \left(\frac{h_{cu}}{h_0}\right)^{(1-m_c)}} \quad (1)$$

with $i \in \{c, n, t\}$ and h_0 = 1 mm. The coefficients k_i were calibrated for the force components in cutting (c), normal (n) and tangential (t) direction of the cutting edge, respectively. This set of coefficients was determined based on the force measurements described in Section 2.2 for each investigated workpiece temperature. Starting from an initial set of coefficients, the force components reconstructed from the simulated undeformed chip thickness were iteratively adjusted using a Broyden–Fletcher–Goldfarb–Shanno (BFGS) optimisation algorithm until the residual between simulated and measured force signal fell below a defined convergence threshold. As the fitting result proved highly sensitive to variations in the exponents m_i, these were fixed throughout the procedure to m_c = 0.25, m_c = 0.2 and m_c = 0.15, so that only the coefficients k_i were adjusted for each workpiece temperature. Combining the temperature-dependent force model with the modal parameters obtained under the corresponding thermal conditions allows the two competing effects introduced to be superimposed and analysed independently within the stability calculation.

3 RESULTS

This section presents the experimental results of the modal analysis, the temperature depended force measurements and the resulting stability predictions obtained from the process simulation, following the structure introduced in Section 2.

3.1 Modal Analysais

Figure 3 shows the measured frequency response functions (FRFs) of the thin-walled workpiece for workpiece temperatures ranging from $T_{Workpiece}$ = −30…20 °C, evaluated over a frequency range up to f = 10,000 Hz. Three distinct natural frequencies can be identified within the investigated range, at approximately $f_1 \approx$ 1500 Hz, $f_2 \approx$ 3000 Hz and $f_3 \approx$ 7250 Hz. Among these, the first bending mode exhibits the highest compliance and therefore dominates the dynamic behaviour of the thin-walled blade, while the second and third modes are comparatively less pronounced. As is characteristic of thin-walled structures, the dynamic compliance of the individual modes varies with the position across the width of the wall, so that the FRF presented here describes the dynamic behaviour at the measurement position defined in Section 2.1. All three identified natural frequencies and their associated dynamic compliances at this position were used as input for the stability calculation.

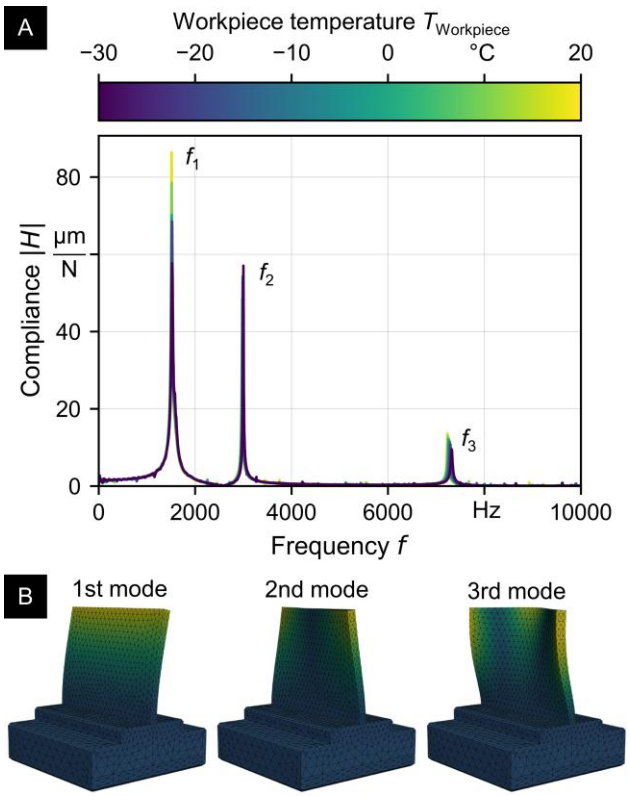


Figure 3. (A) Temperature depended FRF and (B) mode shapes.

Since the first natural frequency represents the dynamically most relevant mode, Figure 4 shows a magnified view of the corresponding frequency range (1000 to 2000 Hz). A clear, continuous shift of the first eigenfrequency toward higher frequencies with decreasing workpiece temperature is visible, accompanied by a pronounced reduction of the peak compliance $|H|$.

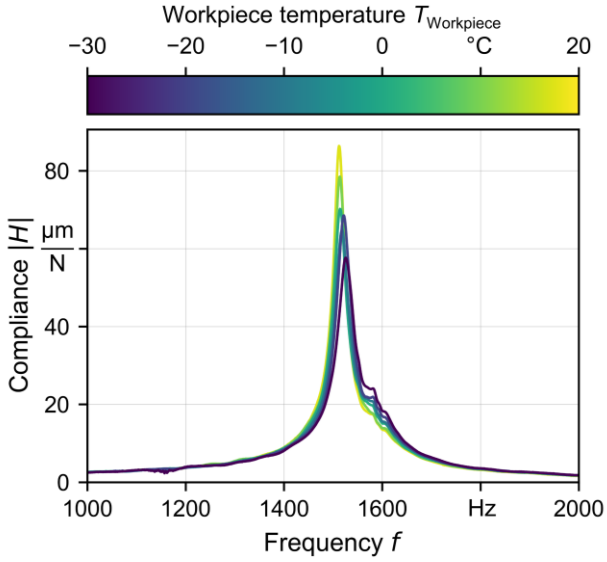


Figure 4. Temperature depended first natural frequency.

For each temperature level, the modal parameters natural frequency, damping ratio and modal mass were extracted from the measured FRFs by means of a fitting procedure (Table 1). The fitted natural frequency increases only slightly with decreasing temperature, from f_1 = 1512.89 Hz at 20 °C to f_1 = 1528.66 Hz at −20 °C, corresponding to a relative increase of about 1.0 %. The identified modal mass remains nearly constant across the investigated temperature range (m = 0.0082-0.0086 kg), since

neither the mass of the specimen nor the mass of the comparatively thin dry ice layer changes significantly with the applied cooling. According to the relationship $f \propto \sqrt{(k/m)}$ between the natural frequency f, the modal stiffness k and the modal mass m, a shift in frequency at near constant modal mass can only result from a corresponding change in modal stiffness k. The observed upward shift of the first eigenfrequency with decreasing temperature therefore directly indicates an increase in the dynamic stiffness of the thin-walled component, consistent with the increase of the material's young's modulus introduced in Section 1. At the same time, the decreasing compliance of the first eigenfrequency with decreasing temperature confirms the stiffening effect quantitatively, as a lower peak compliance directly corresponds to a higher effective structural stiffness at resonance. In contrast, the fitted modal damping coefficient γ increases markedly and monotonically with decreasing temperature, from $\gamma = 139.8\ s^{-1}$ at 20 °C to $\gamma = 248.8\ s^{-1}$ at −20 °C, an increase of nearly 80 % across the investigated range. Since the peak amplitude of a resonance is often governed primarily by damping rather than by stiffness, this pronounced rise in damping, rather than the comparatively small change in modal stiffness, is identified as the main contributor to the reduction in peak compliance observed with decreasing temperature.

The identified damping ratio must, however, be interpreted with some caution with regard to the applied cooling strategy. Owing to the low nozzle exit temperature of the CO_2 jet, a fraction of the expanded CO_2 can additionally desublimate directly on the cooled workpiece surface, forming a thin layer of solid CO_2 dry-ice. Since this dry-ice layer is mechanically less stiff than the aluminium blade, it may introduce an additional, temperature-dependent frictional or material damping contribution that is superimposed on the structural damping of the workpiece itself. Consequently, part of the observed increase in damping ratio with decreasing temperature cannot be unambiguously attributed to the workpiece material alone and may instead be influenced by the amount and mechanical state of the dry-ice phase present on the surface at the time of excitation.

Temperature [°C]	f [Hz]	m[kg]	γ [s^{-1}]
20	1512.89	0.00863	139.809
10	1514.19	0.00860	162.418
0	1515.08	0.00839	187.746
-10	1518.99	0.00822	208.35
-20	1528.66	0.00824	248.838

Table 1. Modal parameters of the first natural frequency.

3.2 FORCE MEASUREMENT

Since the dynamic response of the measurement chain itself, comprising the dynamometer, the specimen mounting and the ceramic base plates, can be affected by the applied cooling, for instance through a change in the effective screw preload of the clamping caused by thermal contraction, the raw force signals were compensated with a temperature dependent inverse filter prior to further evaluation. For this purpose, the transfer function G_{FF} of the measurement chain was applied in the frequency domain. Figure 5 shows the original and the filtered force signal F_x together with the corresponding amplitude spectra, obtained via Fast Fourier Transform (FFT), and the transfer function G_{FF}. As the FFT illustrates, the natural frequency related resonance of the dynamometer lies well above the frequency range that carries the relevant process force content, such that the inverse filter correction acts only on a frequency band containing a negligible proportion of the process force spectrum. The inverse filter was therefore only applied up to $f = 3000$ Hz. Above this frequency, the dynamometer exceeds its valid measuring range, and applying the inverse filter would artificially amplify high frequency noise rather than physically correct the force signal.

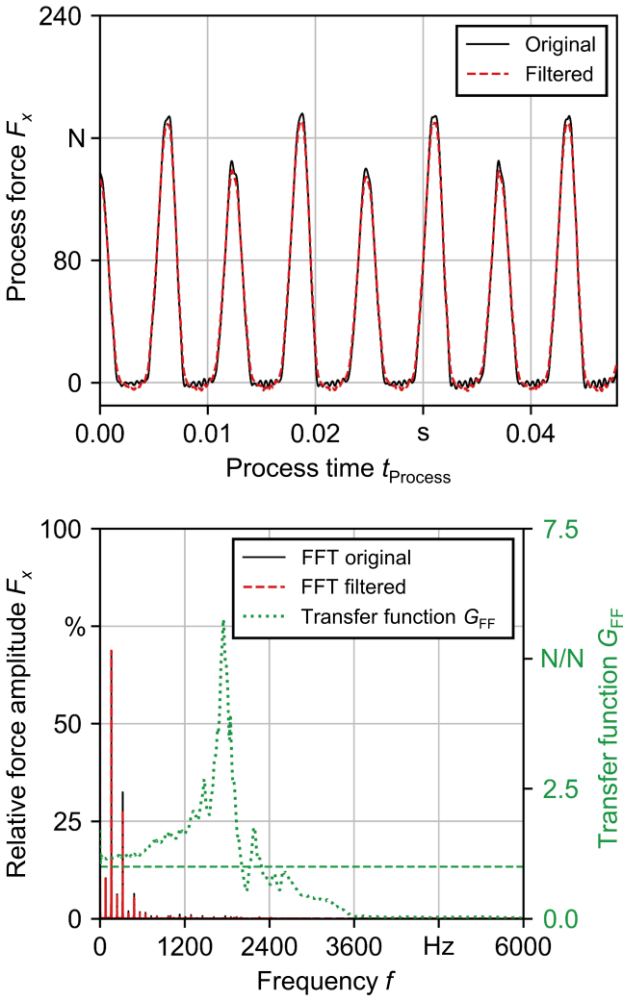


Figure 5. Process Force F_x with the original and the filtered force signal.

The filtered force signals were subsequently evaluated using a peak-picking approach. Owing to the two fluted tool geometry and the applied spindle speed of $n = 5000\ min^{-1}$, the process forces exhibit a periodic pattern with two force pulses per spindle revolution, each corresponding to the engagement of one cutting edge (Figure 6). A clear alternation between the force peak heights of successive engagements can be observed, which is attributed to a runout error of the two-fluted end mill. For every recorded time signal, the local maximum associated with each individual tooth engagement was identified (coloured markers), yielding one force peak per tooth engagement. For each investigated workpiece temperature, 50 individual peaks were extracted per force direction from this stationary window of each of the two independent experiments, providing a sufficiently large sample to characterize both the mean force level and its scatter. Among the three fixed force components, the passive force F_z is by far the smallest under the selected engagement. Under these conditions, the process forces are dominated by the tangential and radial engagement of the

cutting edge, which are reflected in F_x and F_y.

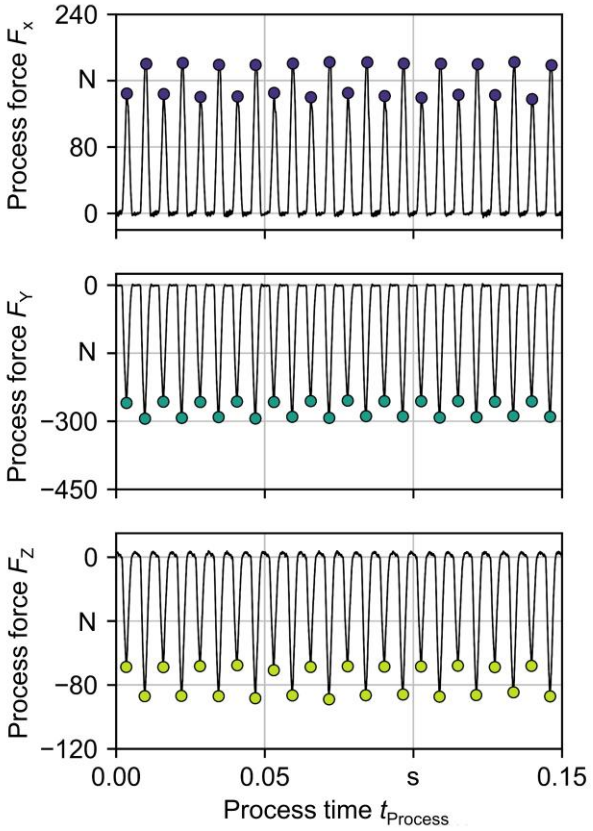


Figure 6. Measured process forces F_x, F_y and F_z, with the extracted force peaks marked for the subsequent evaluation.

Figure 7 shows the extracted force amplitudes as a function of the workpiece temperature. Averaged over the individual tooth engagements evaluated at each temperature level, the mean force amplitudes range from $F_x \approx 158…166$ N, $F_y \approx 272…300$ N and $F_z \approx 75…79$ N across the investigated range from $T_{Workpiece} = -20…20$ °C. In relative terms, this corresponds to a variation of only ±5 % around the respective mean value for all three force components, without a consistent, monotonic trend with temperature: the mean F_y amplitude, for instance, first rises from $F_y = 281$ N at -20 °C to a maximum of $F_y = 300$ N at −10 °C, before decreasing again to $F_y = 272$ N at 20 °C. This comparatively weak sensitivity of the process forces to the workpiece temperature is plausible when the investigated temperature range is compared with the cryogenic conditions typically reported in the literature discussed in Section 1: the pronounced increase in yield strength and flow stress of aluminium alloys at low temperatures is generally reported for substantially lower temperature levels (e.g. down to −196 °C), while the strengthening effect between room temperature and moderately sub-zero temperatures around −20 °C is comparatively small, since the temperature dependence of the flow stress of aluminium alloys is markedly non-linear and becomes pronounced mainly at more extreme cryogenic temperatures [Jin et al. 2024]. Within the investigated temperature window, the resulting excitation force increase therefore appears to be of secondary relevance compared with the pronounced, simultaneously observed increase in structural stiffness described in Section 3.1.

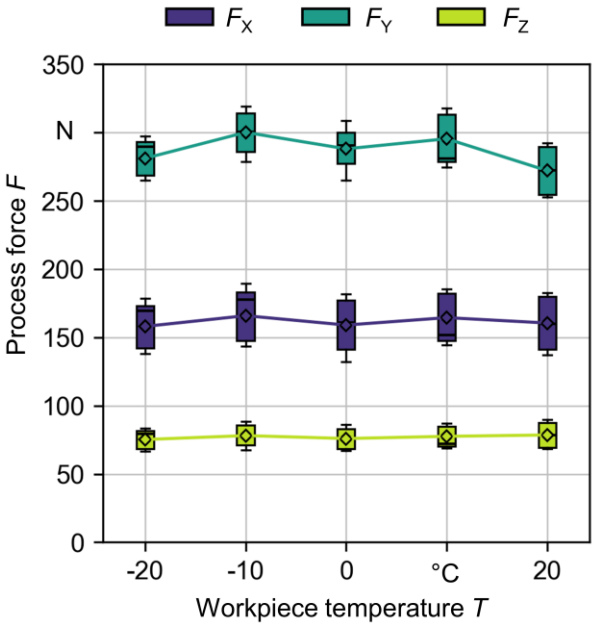


Figure 7. Temperature dependent process forces.

3.3 Simulation

The temperature-dependent Kienzle force model introduced in Section 2.3 was fitted to the force measurements described in Section 3.2 following the same procedure for each investigated workpiece temperature. Since the simulation cannot reproduce the runout induced alternation between the two cutting edges described in Section 3.2, the measured force signals were averaged over the individual tooth engagements prior to the fitting, so that the comparison with the simulation is not biased by this runout effect. Figure 8 shows the resulting comparison between the measured and the simulated process forces for an exemplary workpiece temperature of $T_{Workpiece} = 20$ °C, demonstrating good agreement between simulation and experiment across all three force directions. Table 2 summarizes the resulting temperature-dependent Kienzle force coefficients $k_{c1.1}$, $k_{t1.1}$ and $k_{n1.1}$ for the three investigated workpiece temperatures. Consistent with the comparatively weak temperature dependence of the raw force amplitudes already discussed in Section 3.2, the fitted coefficients likewise vary only slightly across the investigated range and do not follow a monotonic trend with temperature. The specific cutting-force coefficient $k_{c1.1}$ is particularly stable, varying by less than 1 % (683.1-689.4 N/mm²) between 20 °C and −20 °C. The tangential and normal force coefficients $k_{t1.1}$ and $k_{n1.1}$ exhibit a somewhat larger scatter, on the order of 6–11 %, with both reaching a local maximum at 0 °C rather than increasing continuously toward lower temperatures. This pattern is more consistent with scatter arising from the fitting procedure and from the measurement uncertainty already discussed for the process forces (Section 3.2) than with a systematic influence of the workpiece temperature on the underlying material's flow stress.

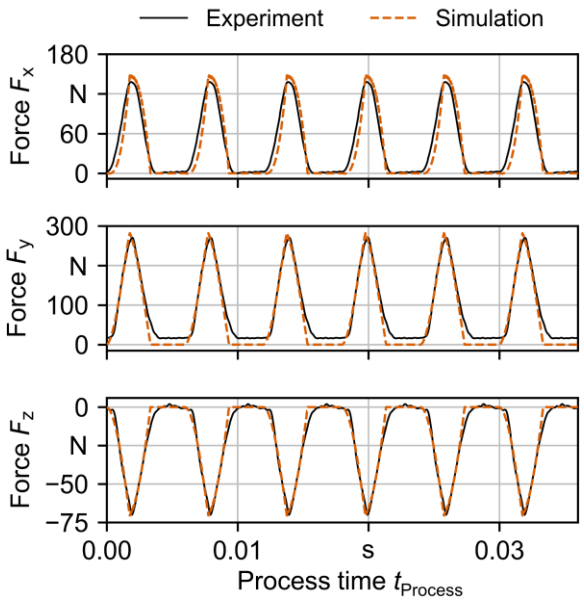


Figure 8. Measured and simulated process force.

This confirms, at the level of the fitted material model, the conclusion drawn in Section 3.2: within the investigated, moderately sub-zero temperature range, the cryogenic cooling of the EN AW-7075 workpiece does not produce a measurable, systematic increase in the specific cutting forces, in contrast to the pronounced strengthening reported in the literature for substantially lower cryogenic temperatures.

Temperature [°C]	$k_{c1.1}$ [N/mm²]	$k_{t1.1}$ [N/mm²]	$k_{n1.1}$ [N/mm²]
20	689.44	199.56	57.09
0	685.69	211.99	63.59
-20	683.12	207.62	57.25

Table 2. Fitted temperature dependent Kienzle force coefficients.

Combining the temperature dependent modal parameters with the fitted Kienzle force model, the geometric-physically based process simulation introduced in Section 2.3 was used to compute the resulting stability limit $a_{p,crit}$ as a function of spindle speed for each investigated workpiece temperature (Figure 9). The stability limits presented here apply to the dynamic properties at the considered measurement position. In thin-walled machining, the dominant dynamic compliance varies along the machining path, both because the relative weighting of the individual modes changes across the width of the wall and because the natural frequencies shift with progressive material removal, so the absolute values of $a_{p,crit}$ are position-dependent. As the objective of this analysis is to isolate the influence of workpiece temperature, the position was kept constant while the temperature was varied, so that the temperature-dependent trend identified here is evaluated on an otherwise identical dynamic basis. Across the investigated range, the predicted stability boundary retains its characteristic lobe shaped structure, with only comparatively small differences between the individual temperature levels. With decreasing temperature, the critical depth of cut increases slightly. Given the negligible and non-monotonic change in modal stiffness identified in Section 3.1, this increase in $a_{p,crit}$ is attributed primarily to the pronounced increase in structural damping rather than to a change in stiffness. In addition, a slight phase shift of the stability lobes along the spindle speed can be observed with decreasing temperature, which follows from the corresponding shift of the first natural frequency of the dominant mode.

Overall, these results indicate that, for the present configuration in which only the CO_2 jet was applied without forming the cryogenic ice-based support structure, the pure cooling of the workpiece does not compromise process stability. On the contrary, the increased structural damping tends to slightly raise the achievable stability limit, while the corresponding increase in excitation force, which had been considered a potentially competing effect in Section 1, remains negligible within the investigated temperature range.

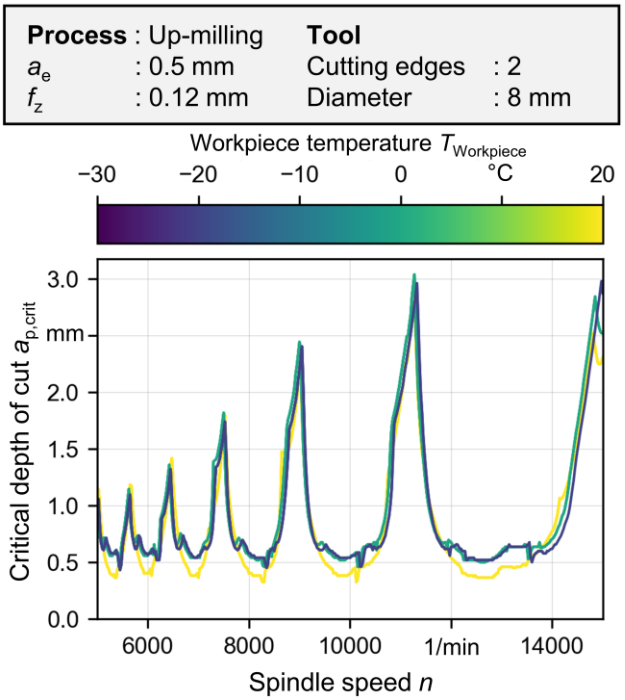


Figure 9. Temperature dependent stability limit.

4 CONCLUSIONS

This study investigated the influence of cryogenic cooling on the process dynamics and stability of milling thin-walled EN AW-7075 components, addressing the competing effects of temperature dependent excitation forces and structural stiffness. For this purpose, an experimental setup combining cryogenic CO_2 cooling with experimental modal analysis and dynamometer-based force measurements was used, together with a geometric-physically based process simulation.

The experimental modal analysis showed that, when CO_2 jet cooling is applied, the first eigenfrequency of the thin-walled specimen shifts only slightly, by about 1 %, between 20 °C and −20 °C, while the corresponding modal stiffness changes only marginally and non-monotonically. In contrast, the modal damping coefficient increased markedly and consistently, by nearly 80 % over the same temperature range, an effect that cannot be fully attributed to the workpiece material alone and may be partly influenced by dry ice formation on the cooled surface. The force measurements and the corresponding Kienzle force model showed that the process forces, and the fitted specific force coefficients derived from them, remain within approximately ±5 % across the investigated temperature range without a systematic, monotonic trend. This is consistent with, and can be explained by, the fact that the pronounced increase in yield strength typically reported for aluminium alloys under cryogenic conditions occurs mainly at substantially lower temperatures than those investigated here. The fitted specific cutting-force coefficient $k_{c1.1}$ was found to be in good agreement

with corresponding literature reference value for the investigated EN AW-7075 alloy.

Combining these temperature dependent modal and force models within the process simulation showed that the resulting stability limit retains its characteristic lobe-shaped structure across the investigated temperature range, with only a slight increase in the critical depth of cut — attributable primarily to the increased damping and a minor phase shift of the lobes associated with the eigenfrequency shift. Consequently, within the investigated range, cooling the workpiece with the CO_2 jet alone, without applying the additional ice-based support structure, was found to have no adverse effect on process stability and may even provide a modest stabilizing benefit through increased damping. These findings provide an important reference case for the interpretation of the fully lubricant ice supported configuration, in which the additional ice layer provides both geometric support and a further increase in damping on top of the effects identified here for pure CO_2 cooling.

Since the CO_2-based cooling used in this study can lead to the formation of dry-ice or frost on the workpiece surface, future work should employ an alternative cooling strategy, for example a Peltier-element-based cooling plate, which does not produce such a surface layer, to directly decouple the observed damping contribution from this effect, without requiring any additional modelling.

ACKNOWLEDGMENTS

This research was funded by the German Research Foundation (DFG, Deutsche Forschungsgemeinschaft) – project number 515938217.

DECLARATION ON THE USE OF ARTIFICIAL INTELLIGENCE

During the preparation of this work the authors used claude.ai in order to improve the readability of the paper. After using this tool, the authors reviewed and edited the content as needed and take full responsibility for the content of the publication.

REFERENCES

[Bian et al. 2025] Bian, Y. et al. Investigation on surface quality of milling Ti6Al4V alloy thin-walled parts based on ice fixation. The International Journal of Advanced Manufacturing Technology, 2025, Vol. 136, 5-6, pp. 2821–2834. ISSN 0268-3768.

[Herranz et al. 2005] Herranz, S. et al. The milling of airframe components with low rigidity: A general approach to avoid static and dynamic problems. Proceedings of the Institution of Mechanical Engineers, Part B: Journal of Engineering Manufacture, 2005, Vol. 219, No. 11, pp. 789–801. ISSN 0954-4054.

[Jaeger et al. 2020] Jaeger, E. et al. Cryogenically Applied Support and Damping Structures for Chatter Suppression in the Machining of Thin-Walled Components. SSRN Electronic Journal, 2020.

[Jaquet et al. 2026] Jaquet, S. et al. Process Stabilization through Cryogenically Generated Support Structures and its Impact on Dimensional Accuracy in Milling Thin-Walled Components. Procedia CIRP, 2026, Vol. 141, pp. 55–60. ISSN 22128271.

[Jin et al. 2024] Jin, M. et al. Cryogenic Deformation Behaviour of Aluminium Alloy 6061-T6. Metals and Materials International, 2024, Vol. 30, No. 6, pp. 1492–1504. ISSN 1598-9623.

[Kienzle 1952] Kienzle, O. Die bestimmung von kräften und leistungen an spanenden werkzeugen und werkzeugmaschinen. VDI-Z, 1952, No. 94.11.

[Korkmaz and Gupta 2024] Korkmaz, M.E. and Gupta, M.K. A State of the Art on Cryogenic Cooling and Its Applications in the Machining of Difficult-to-Machine Alloys. Materials (Basel, Switzerland), 2024, Vol. 17, No. 9. ISSN 1996-1944.

[Liu et al. 2021] Liu, H. et al. The influence of ice-based fixture on suppressing machining-induced deformation of cantilever thin-walled parts: a novel and green fixture. The International Journal of Advanced Manufacturing Technology, 2021, Vol. 117, 1-2, pp. 329–341. ISSN 0268-3768.

[Möhring et al. 2025] Möhring, H.-C. et al. Fixtures and workpiece clamping systems in machining. CIRP Annals, 2025, Vol. 74, No. 2, pp. 945–969. ISSN 00078506.

[Munoa et al. 2016] Munoa, J. et al. Chatter suppression techniques in metal cutting. CIRP Annals - Manufacturing Technology, 2016, Vol. 65, No. 2, pp. 785–808. ISSN 00078506.

[Naimon et al. 1975] Naimon, E.R. et al. Low-temperature elastic properties of four wrought and annealed aluminium alloys. Journal of Materials Science, 1975, Vol. 10, No. 8, pp. 1309–1316. ISSN 0022-2461.

[Platt et al. 2020] Platt, T. et al. Conduction-Based Thermally Assisted Micromilling Process for Cutting Difficult-to-Machine Materials. Journal of Manufacturing and Materials Processing, 2020, Vol. 4, No. 2, p. 34.

[Quintana and Ciurana 2011] Quintana, G. and Ciurana, J. Chatter in machining processes: A review. International Journal of Machine Tools and Manufacture, 2011, Vol. 51, No. 5, pp. 363–376. ISSN 08906955.

[Ranjbar et al. 2026] Ranjbar, S. et al. Effects of cryogenic cooling on cutting temperature and surface roughness in turning of AA7075 aluminum alloy. Scientific reports, 2026, Vol. 16, No. 1.

[Wang et al. 2025] Wang, C. et al. Design of a novel ice-based fixture and its application in the machining of integrated structural thin-walled components. Journal of Manufacturing Processes, 2025, Vol. 149, pp. 852–867. ISSN 15266125.

[Wiederkehr et al. 2018] Wiederkehr, P. et al. Point-based tool representations for modeling complex tool shapes and runout for the simulation of process forces and chatter vibrations. Advances in Manufacturing, 2018, Vol. 6, No. 3, pp. 301–307. ISSN 2095-3127.

[Zhu et al. 2018] Zhu, L. et al. Light-weighting in aerospace component and system design. Propulsion and Power Research, 2018, Vol. 7, No. 2, pp. 103–119. ISSN 2212540X.

CONTACTS:

Simon Jaquet M. Sc.
TU Dortmund University, Institute of Machining Technology
Baroper Str. 303, Dortmund, 44227, Germany
+49 231 755 8045, simon.jaquet@tu-dortmund.de

LICENSE CREATIVE COMMONS:

The article is published under the terms and conditions of the Creative Commons Attribution 4.0 International License (CC BY 4.0).